Available online at www.sciencedirect.com
ScienceDirect
ELSEVIER
International Journal of Multiphase Flow 32 (2006) 1037–1054
International Journal of Multiphase Flow
www.elsevier.com/locate/ijmulflow

Effects of vibrations on particle motion near a wall: Existence of attraction force

Samer Hassan [a,1], Tatyana P. Lyubimova [b], Dmitry V. Lyubimov [c], Masahiro Kawaji [a,*]

[a] Department of Chemical Engineering and Applied Chemistry, University of Toronto, Toronto, Ont., Canada M5S 3E5
[b] Institute of Continuous Media Mechanics UB, RAS, Perm, Russia
[c] Perm State University, Theoretical Physics Department, Perm, Russia

Received 26 September 2005; received in revised form 16 May 2006

Abstract

The effects of small vibrations on a particle oscillating near a solid wall in a fluid cell, relevant to material processing such as crystal growth in space, have been investigated experimentally and theoretically. Assuming the boundary layer around the particle to be thin compared to the particle radius at high vibration frequencies, an inviscid fluid model was developed to predict the motion of a spherical particle placed near a wall of a rectangular liquid-filled cell subjected to a sinusoidal vibration. Under these conditions, a non-uniform pressure distribution around the particle results in an average pressure that gives rise to an attraction force. Theoretical expressions for the attraction force are derived for the particle vibrating normal to and parallel with the nearest cell wall. The magnitude of this attractive force has been verified experimentally by measuring the motion of a steel particle suspended in the fluid cell by a thin wire. Experiments performed at high frequencies showed that the mean particle position, when the particle is brought near a cell wall, shifts towards the same wall, and is dependent on the cell amplitude and frequency, particle and fluid densities.

Keywords: Hydrodynamics; Pulsational flow; Vibration frequency and amplitude; Particle motion; Attraction force; Induced flow; Fluid cell; Wall effect

1. Introduction

Advanced materials such as semi-conductor and protein crystals can be produced under microgravity where the effect of density variation within a fluid system becomes unimportant and buoyancy-induced motion and sedimentation are suppressed. However, many semi-conductor and protein crystal growth experiments conducted in the past aboard the Space Shuttle and Mir Space Station have yielded unexpected results possibly

* Corresponding author. Tel.: +1 416 978 3064; fax: +1 416 978 8605.
E-mail address: kawaji@ecf.utoronto.ca (M. Kawaji).
[1] Tel.: +416 978 6727; fax: +416 978 8605.

0301-9322/$ - see front matter
doi:10.1016/j.ijmultiphaseflow.2006.05.008

due to small vibrations existing on the space platforms called g-jitter. These vibrations could alter the fluid behavior under microgravity which may lead to different crystal properties. Space platforms could provide an ideal environment to conduct diffusion-controlled experiments if g-jitter can be reduced.

The overall objective of this paper is to better understand the effects of small vibrations on particle–fluid systems relevant to material processing under microgravity and on Earth. More specifically, the motion of a solid particle in a sinusoidally-vibrated semi-infinite fluid cell has been investigated both theoretically and experimentally. The fluid cell is filled with an inviscid liquid, and the particle is induced to oscillate near one of the cell walls by cell vibration. The particle oscillation amplitude is theoretically predicted and compared with experimental data obtained over a wide range of vibration conditions. In the present paper, a systematic series of experimental and theoretical investigations will be described to show the existence of a vibration-induced attraction force when the particle oscillates near a cell wall in both perpendicular and parallel directions with respect to the nearest wall.

A number of studies have been reported on flow-induced vibrations of solid particles. Some works include particles undergoing a sinusoidal motion in an otherwise quiescent fluid. Other works include the interaction force between two pulsating spheres in a fluid cell or the behavior of the particle near a wall when it is released in a fluid cell under a gravitational acceleration field. However, the reverse situation of vibration-induced particle and fluid motion, in which the particle immersed in a fluid and vibrated near a cell wall in a semi-infinite cell, has not yet been fully explored and tackled by any physical experiment. Some results of the previous theoretical and experimental studies relevant to this work are briefly reviewed first, followed by descriptions of the experimental and theoretical investigations performed in this work.

Stokes (1851) derived, by eliminating the inertia terms in all his calculations, the expressions for the forces acting on a particle by the surrounding fluid subjected to harmonic motion. Basset (1888) and Boussinesq (1885) expanded the expressions for the forces acting on a sphere in an arbitrary accelerating motion where they also neglected the non-linear terms in order to simplify the Navier–Stokes equations. Leahy (1884) investigated theoretically the mutual action of two small spheres in an elastic medium. He found that the repulsive or attraction force varies inversely with the square of the distance between them if the third or higher-order terms are neglected. However, when he included the terms of the third order in the expression for the particle displacement, he found that the force is inversely proportional to the cube of the distance between the two spheres. Hicks (1880) determined the coefficients of the velocities in the expression for the kinetic energy in the form of an infinite series, when two spheres are moving in an infinite liquid with a uniform speed along the line joining their centers of mass. His method was not very effective and only approximate solutions were attained. Basset (1887) gave an approximate solution using the transformation of spherical harmonics.

Other important studies had been performed to determine the terminal velocities of a spherical particle in a vertically oscillating liquid. Among these studies were the ones published by Jameson and Davidson (1966), Baird et al. (1967) and Ikeda and Yamasaka (1989). Molinier et al. (1971) dealt with the study of the motion of a sphere in a column where there is a circulation of a viscous oil. Eames et al. (1996) studied the displacement of an inviscid fluid by a sphere moving away from a wall at a constant speed; in their paper, the fluid displacement by a solid body moving away from a wall was calculated, using the flow around a sphere. Milne-Thomson (1968) derived an analytical expression for the hydrodynamic force acting on a particle in a quiescent, inviscid fluid at a distance H from an infinite wall. Using the method of Lagrange, he derived an expression for the horizontal force acting on the particle in the x-direction normal to the nearest wall. He concluded that if a spherical particle is moving in the x-direction directly towards the wall, a force towards the wall is required to maintain a constant speed. Hence, a force opposite in direction is apparently induced to repel the sphere from the wall. Unfortunately, he did not include a mathematical analysis of the particle–fluid system subjected to an external excitation.

The important reference that summarizes to a certain extent some works on particle–fluid interaction was published by Clift et al. (1978) in which all the main studies up to 1978 for the motion of drops, bubbles and particles are covered. It covers flows at low and high Reynolds numbers, the drag force induced and the wall effects on the particle motion. Unfortunately, there is no mathematical expression for the vibration effect on the motion of a particle vibrating near a wall in a fluid cell. Chelomey (1983) performed some experiments on a solid particle immersed in a liquid-filled container subjected to vibrations and concluded that under certain conditions, non-uniform forces arise with zero-mean values acting on the particle. In his work, Chelomey

(1983) claimed that there were induced forces during vibration which could result in a paradoxical behavior of bodies in an oscillating liquid; bodies of greater density than the surrounding fluid would emerge at the top, whereas light bodies would move downward against the force of gravity.

Houghton (1961) analyzed the non-linear drag (Newton's law) force on free particles in a sinusoidal velocity field leading to the Mathieu equation, where he found that stable particle trajectories may occur in certain ranges of amplitude and frequency. Houghton did not include any finite cell effect in his study, and he did not derive any analytical equation showing the near-wall effect on the particle's sinusoidal motion. Li et al. (1993) used a successive images method to determine the velocity potential and hence the interacting force on two spheres moving with steady velocities normal to the line joining their centers of mass. The motion of high Reynolds number bubbles in inhomogeneous flow has been predicted by Magnaudet and Eames (2000) but their analysis did not include any wall effect. Magnaudet (2003) recently studied the motion of a particle near a wall at a finite Reynolds number, but this study did not incorporate any effect of vibration near a cell wall.

A recent study on vibration-induced particle motion in an infinite fluid cell, has been presented by Hassan et al. (2006a). In their study, a theoretical model of a spherical particle vibrating in a large fluid cell was derived assuming an inviscid fluid and irrotational flow. They also measured the amplitude of a spherical particle suspended in a rectangular water-filled cell by a thin wire and subjected to sinusoidal vibrations. The infinite cell model was shown to predict the measured particle amplitudes well. A semi-infinite cell model for a particle vibrating normal to a cell wall was also developed by Hassan et al. (2006b) where the effect of the cell width was studied experimentally and theoretically. In deriving an expression for the particle amplitude, however, they did not consider the effect of an attraction force that can develop when the particle is vibrating very close to a solid wall.

The present paper is related to the applications of the acoustic streaming phenomena reviewed recently by Riley (2001). Examples of these applications include the use of unidirectional streaming flow to measure the adsorption coefficients of common liquids, and reduction of the heating effect produced by the impact of an ultrasonic beam on a bone tissue. Riley (2001) expanded the vorticity equation at the leading order of $\varepsilon = U_0/\omega R_0$ where ε is the expansion parameter, U_0 is the velocity amplitude associated with fluctuations, ω is the angular frequency of vibration, and R_0 is the particle radius. He found that the vorticity has a non-zero time average value, indicating that steady streaming is induced in the fluid at the leading order of expansion. He stated that for a spherical particle oscillating in a low viscosity fluid at rest with the kinematic viscosity, $\nu \ll \omega R_0^2$, the flow is composed of two separate patterns. The first is an oscillatory flow at the leading order of expansion in the bulk of the fluid and is irrotational. The second flow is a steady mean flow reaching the edge of the boundary layer (Stokes layer) and streaming in the bulk of the fluid. The first and second flow patterns are related, respectively, to the oscillatory particle motion and the particle drift investigated in the present work.

From the above studies, it is evident that the existence of an attraction force has not been investigated in detail when the particle is vibrating in a sinusoidal motion near a fluid cell wall. Thus, the objective of this paper is to investigate theoretically and experimentally the magnitude and dependence of the attraction force on various parameters relevant to the vibration-induced motion of a solid particle in a fluid cell.

2. Experimental apparatus

The experimental apparatus consisted of a test section, a linear translation stage, and a video camera/recording system as shown in Fig. 1. Each of the major components is described below in detail. The test section was mounted on a linear stage which was installed on a vibration-isolating optical table to be totally isolated from external vibrations, and this was checked by a calibrated accelerometer.

A PC-controlled mechanical translation stage was used to vibrate the fluid cell with sub-micron resolution and repeatability at frequencies below 7 Hz. It was controlled to move the fluid cell horizontally with a specified amplitude and frequency in a near sinusoidal manner. For higher frequency vibrations (>7 Hz), an air bearing stage driven by an electromagnetic actuator (Labworks Inc., Model ET-132-2) was used that minimized small vibrations in the other two directions. The cell motion was also measured using a laser displacement sensor (Keyence Model ILD 1401-5) with a 1 μm resolution.

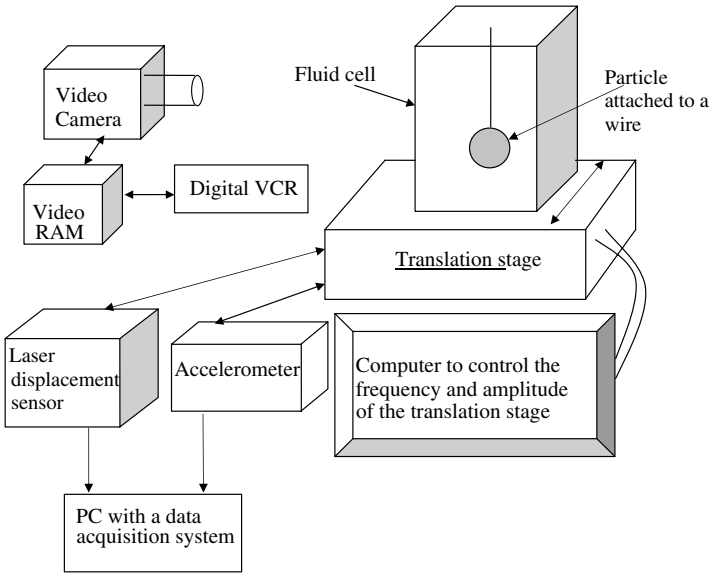

Fig. 1. Experimental set-up.

The test section was a water-filled rectangular vessel made of smooth and transparent acrylic plates. The internal dimensions of the fluid cell were 50.0 mm (W) × 50.0 mm (L) and 110 mm (H). In order to vary the width of the cell and to study the wall proximity effects on the particle motion, six grooves were cut on two opposite side walls to enable insertion of up to three 6.0-mm thick acrylic plates. A spherical steel particle (density = 7.83 g/cm^3, diameter = 12.7 mm) was suspended in the fluid cell with a thin platinum wire of 125 μm diameter and 76 mm length. The effects of the wire diameter and length on the particle motion had been studied previously by Hassan et al. (2006a), and the wire diameters less than 150 μm had been determined to exert no influence on the vibration-induced particle motion amplitude. The fluid cell was completely filled with distilled and degassed water, which has relatively low viscosity ($\mu = 10^{-3}$ kg/m s at 20 °C and 1 atm) and may be considered as inviscid from a theoretical point of view.

A CCD video camera (Hitachi D.S.P. VK C-370 or a Megaplus high speed camera) with an interchangeable lens was used to capture the particle motion with sufficient magnification. The edge of the particle was captured at 30 frames per second with the Hitachi CCD camera and at 125 frames per second with the Megaplus camera for cell vibration frequencies below 7 Hz and above 7 Hz, respectively. The shutter speed was set at 1/1000 s^{-1} to obtain sharp images. The particle edges recorded in a digital video tape were analyzed using an image analysis program. In total, 255 frames of particle edges captured over 8.64 s or 2.0 s were analyzed frame by frame for each run, and the data were entered into a spreadsheet to calculate the particle oscillation amplitude and frequency.

In order to investigate the wall proximity effects, four small holes were drilled through the top cover plate and the end of the platinum wire was fixed to one of the holes at different positions from the nearest wall. By inserting one or more 6.0 mm-thick plates into the grooves, the distance between the center of the particle and the nearest wall, H, could be varied from 8.0 mm to 17.0 mm. The vibration amplitude, a, was set at 1.0 mm, and the vibration frequency was increased from 2 Hz to 20 Hz over small increments.

The above procedure was repeated for different values of H to detect any wall-proximity effect. Before the data were collected, the system was run for at least 5 min to allow the particle and fluid motions to become stable under the operating conditions. The video camera was then used to capture the image of the edge of the oscillating particle. A back light was placed far from the fluid cell to avoid any heating effect. The particle image data were recorded on a mini-DV video-cassette by means of a digital VCR (JVC Model AG-7355) for the 30 fps camera, or saved directly in the PC hard drive for the 125 fps camera.

The images of the particle edge were analyzed using an edge detection program designed to calculate the edge coordinates in each frame. A pixel to mm conversion factor was obtained by lowering a platinum wire

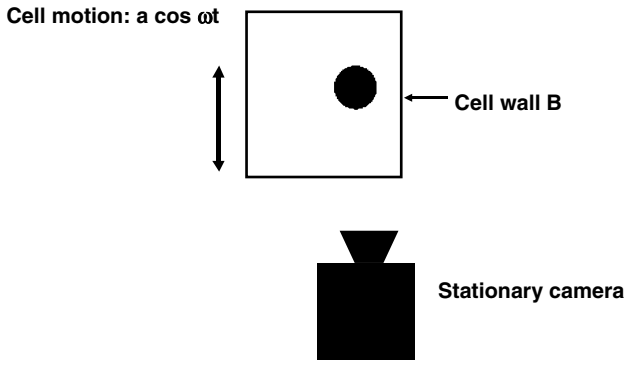

Fig. 2. Experimental detection of the attraction force.

of known diameter to the bottom of the fluid cell and recording its image. Then by using the same image analysis program, the wire diameter in pixels was calculated and a conversion factor was computed.

The fluid cell was mounted on a platform fixed to the translation stage while the video camera was either fixed on the same platform or mounted on an optical table. In the former configuration, the video camera recorded the particle motion in the cell's frame of reference, while in the latter, the camera captured the particle motion in the fixed frame of reference. When the particle motion was parallel to the nearest wall, the video camera was oriented parallel with the plane of the particle oscillation as shown in Fig. 2 to detect the mean attraction force, which would cause the plane of the particle oscillation to drift towards the nearest wall.

3. Theoretical analysis of particle oscillation normal to a container wall

To analytically investigate the wall-proximity effect on the particle motion and the existence of the attraction force, an inviscid fluid model is developed below for a particle vibrating in a plane normal to a cell wall. This model predicts a non-uniform pressure distribution around the particle, which can be integrated around the particle surface to yield an expression for a mean attraction force. This force will be shown to be dependent on the cell vibration frequency and amplitude, the liquid and particle densities and a ratio of the distance between the center of the particle and the cell wall to the particle radius, H/R_0. To verify the attraction force expression derived, experimental data will be compared with the shift in the mean particle position predicted by a force balance on the particle oscillating in an inviscid fluid.

The use of an inviscid fluid assumption can be justified by examining the ratio of the combined inertial forces of the particle and fluid to the viscous force, which is proportional to $\frac{(\rho_L+\rho_S)}{\rho_L}\frac{R_0}{\delta_S}$, where ρ_L is the fluid density, ρ_S is the particle density and δ_S is the thickness of the viscous Stokes layer. In the present work, δ_S of about 0.18 mm for water at a cell vibration frequency of 10 Hz and R_0 of 6.35 mm, so the ratio of inertial to viscous forces is large and a potential flow can be assumed to exist outside the viscous Stokes layer. From another perspective, the Reynolds number in the present work can be given by $\frac{A_p\omega D_0}{\nu}$ where A_p is the particle amplitude, ω is the angular frequency of particle vibration, and D_0 is the particle diameter. For a cell vibration frequency of 10 Hz and for a steel particle of radius 6.35 mm used in this work, the particle amplitude in water is measured to be 830 μm and the Reynolds number is about 660, which is high enough to justify the inviscid fluid assumption.

Thus, in the following derivation for a particle–fluid system subjected to a sinusoidal acceleration under zero-gravity, the viscous terms are assumed to be negligible compared to inertia terms. Furthermore, based on the equation for the rate of particle rotation near a wall given by Happel and Brenner (1983), the particle rotation rate was estimated to be very small even for the maximum particle velocity measured and minimum particle–wall distance used in the experiment. Thus, the effect of particle rotation was also neglected.

It is convenient to write down the momentum and continuity equations in the particle's frame of reference as follows:

$$\frac{\partial \vec{\boldsymbol{v}}}{\partial t} + (\vec{\boldsymbol{v}}.\nabla)\vec{\boldsymbol{v}} = -\frac{\nabla p}{\rho_{\mathrm{L}}} - \frac{\mathrm{d}\vec{\boldsymbol{u}}}{\mathrm{d}t} \tag{1}$$

$$\operatorname{div} \vec{\boldsymbol{v}} = 0 \tag{2}$$

where $\vec{\boldsymbol{u}}$ is the particle velocity vector in the laboratory frame of reference, $\vec{\boldsymbol{v}}$ is the fluid velocity vector relative to the particle, p is pressure, ρ_{L} is liquid density and t is time. The pulsational motion of the fluid is considered as a potential flow,

$$\vec{\boldsymbol{v}} = \nabla\varphi \tag{3}$$

where φ is a harmonic function that satisfies the Laplace equation,

$$\Delta\varphi = 0 \tag{4}$$

The impermeability boundary conditions at the particle surface and the container walls are respectively given by

$$\left.\frac{\partial\varphi}{\partial n}\right|_{\mathrm{s}} = 0 \tag{5}$$

$$\left.\frac{\partial\varphi}{\partial n}\right|_{\mathrm{W}} = w_{\mathrm{n}} - u_{\mathrm{n}} \tag{6}$$

where n indicates the outward direction normal to the particle surface, and w_{n} and u_{n} are the components of the wall and particle velocities in the normal direction.

It is necessary to consider at this stage small amplitude vibrations. By omitting the non-linear terms in Eq. (1), the pulsational pressure $\tilde{p}$ can be obtained by integrating the same equation as

$$\tilde{p} = -\rho_{\mathrm{L}}\left(\frac{\partial\varphi}{\partial t} + \vec{\boldsymbol{u}}\cdot\vec{\boldsymbol{r}}\right) \tag{7}$$

where $\vec{\boldsymbol{r}}$ is the fluid element's position with respect to the particle. The equation for the pulsational motion of the particle is given by

$$m\frac{\partial\vec{\boldsymbol{u}}}{\partial t} = -\oint \tilde{p}\,\overrightarrow{\mathbf{d}\boldsymbol{S}} \tag{8}$$

where m is the particle mass, and $\overrightarrow{\mathbf{d}\boldsymbol{S}}$ is a vector element of area $\mathrm{d}S$ oriented outward from the center of the sphere.

Substituting Eq. (7) into Eq. (8), we obtain

$$m\frac{\partial\vec{\boldsymbol{u}}}{\partial \mathrm{t}} = \rho_{\mathrm{L}}\oint \frac{\partial\varphi}{\partial t}\overrightarrow{\mathbf{d}\boldsymbol{S}} + \rho_{\mathrm{L}}V\frac{\mathrm{d}\vec{\boldsymbol{u}}}{\mathrm{d}t} \tag{9}$$

where V is the volume of the sphere. If we introduce the particle density, Eq. (9) can be written as

$$(\rho_{\mathrm{S}} - \rho_{\mathrm{L}})V\frac{\mathrm{d}\vec{\boldsymbol{u}}}{\mathrm{d}t} = \rho_{\mathrm{L}}\oint \frac{\partial\varphi}{\partial t}\overrightarrow{\mathbf{d}\boldsymbol{S}} \tag{10}$$

We restrict this analysis to the case where both the container and particle move along the unit vector $\vec{\boldsymbol{i}}$. Thus,

$$\vec{\boldsymbol{u}} = u\vec{\boldsymbol{i}} \tag{11}$$

and

$$\vec{\mathbf{w}} = w\vec{\boldsymbol{i}} \tag{12}$$

It is convenient to separate the time domain from the spatial coordinates using the separation of variables method. Hence, let

$$\varphi = (w-u)(\vec{\boldsymbol{i}}\cdot\vec{\boldsymbol{r}} + \Phi) \tag{13}$$

where the dimensionless function Φ is independent of time and has to satisfy the conditions from Eqs. (4)–(6), respectively as follows:

$$\Delta\Phi = 0 \tag{14}$$

$$\left.\frac{\partial\Phi}{\partial n}\right|_{\mathrm{s}} = -i_{\mathrm{n}} \tag{15}$$

$$\left.\frac{\partial\Phi}{\partial n}\right|_{\mathrm{w}} = 0 \tag{16}$$

where i_{n} is the component of the vector $\vec{\boldsymbol{i}}$ in the normal direction. Hence, the problem now does not contain time.

Substituting Eqs. (11)–(13) into Eq. (10), we obtain

$$(\rho_{\mathrm{S}} - \rho_{\mathrm{L}})V\frac{\mathrm{d}\vec{\boldsymbol{u}}}{\mathrm{dt}} = \rho_{\mathrm{L}}\oint\left(\frac{\partial w}{\partial t} - \frac{\partial u}{\partial t}\right)(\vec{\boldsymbol{i}}\cdot\vec{\boldsymbol{r}} + \Phi)\,\overrightarrow{\mathbf{d}\boldsymbol{S}} \tag{17}$$

Solving (17) for the scalar velocity u yields,

$$u = \rho_{\mathrm{L}} w\left(\frac{V + \vec{\boldsymbol{i}}\oint\Phi\,\overrightarrow{\mathbf{d}\boldsymbol{S}}}{\rho_{\mathrm{S}}V + \rho_{\mathrm{L}}\vec{\boldsymbol{i}}\oint\Phi\,\overrightarrow{\mathbf{d}\boldsymbol{S}}}\right) \tag{18}$$

Eq. (18) can be represented as

$$u = Gw \tag{19}$$

in which G is expressed by

$$G = \frac{1+\alpha}{\frac{\rho_{\mathrm{S}}}{\rho_{\mathrm{L}}} + \alpha} \tag{20}$$

where

$$\alpha = \frac{\vec{\boldsymbol{i}}\oint\Phi\,\overrightarrow{\mathbf{d}\boldsymbol{S}}}{V} \tag{21}$$

If we time-average the momentum Eq. (1) over one vibration period, accounting for the pulsational velocity field, Eqs. (3) and (4), and the sinusoidal motion of the particle, the average pressure, $\bar{p}$, can be obtained as

$$\overline{p} = -\frac{\rho_{\mathrm{L}}}{2}(\nabla\varphi)^2 \tag{22}$$

using the fact that the average of a sinusoidal motion over one period is zero. Substituting Eq. (13) into (22) gives the average pressure as

$$\overline{p} = -\frac{1}{2}\rho_{\mathrm{L}}\overline{w^2}(1-G)^2(\vec{\boldsymbol{i}} + \nabla\Phi)^2 \tag{23}$$

where $\overline{w^2}$ is the average of the instantaneous velocity squared over one oscillation period.

Finally, the average force acting on the particle can be calculated by integrating the average pressure from Eq. (23) around the particle. Hence,

$$\vec{F} = -\oint\bar{p}\,\overrightarrow{\mathbf{d}\boldsymbol{S}} \tag{24}$$

$$\vec{F} = -\frac{1}{2}\rho_{\mathrm{L}}\overline{w^2}\frac{(\rho_{\mathrm{S}} - \rho_{\mathrm{L}})^2}{(\rho_{\mathrm{S}} + \alpha\rho_{\mathrm{L}})^2}N\vec{\boldsymbol{i}} \tag{25}$$

where N is expressed by

$$N = \vec{\boldsymbol{i}}\oint(\vec{\boldsymbol{i}} + \nabla\Phi)^2\,\overrightarrow{\mathbf{d}\boldsymbol{S}} \tag{26}$$

The above analysis is simplified if the particle has a spherical shape with a radius R_0. Expression (21) would then be given by

$$\alpha = \frac{3}{2R_0} \oint \Phi x \, dx \tag{27}$$

where $x = \cos\theta$ is the polar angle calculated from the direction of the unit vector, $\vec{i}$. To solve Eqs. (26) and (27), the function Φ has to be expressed in a certain form to satisfy the Laplace equation. Using a spherical harmonics approach, Φ can be written as

$$\Phi = A_1' \frac{x}{r^2} + A_2' \frac{3x^2 - 1}{r^3} - A_1' \frac{y}{r_1^2} + A_2' \frac{3y^2 - 1}{r_1^3} \tag{28}$$

where $r_1 = \sqrt{4H^2 + 4Hrx + r^2}$ and $y = \frac{(2H + rx)}{r_1}$. Here, r, and r_1 are the distances from the particle and its image to any point in the fluid in the cell, H is the distance between the center of mass of the particle and the nearest wall, as shown in Fig. 3.

A solution of Eq. (28) satisfies the Laplace equation and the boundary conditions at the rigid container wall, but it is impossible to satisfy exactly the boundary conditions on the particle surface. Thus, as long as the particle does not collide with the wall, a relatively large distance between the particle and the wall, H, compared to the particle radius, R_0, will be considered in the following analysis. It will be seen that by properly selecting the constants A_1' and A_2', Eq. (28) can satisfy the boundary conditions with accuracy not worse than the fourth order with respect to (R_0/H).

By using the particle radius as the length scale, Eq. (28) can be non-dimensionalized as

$$\Phi = A_1 \frac{x}{r^2} + A_2 \frac{3x^2 - 1}{r^3} - A_1 \eta^2 \frac{y}{r_2^2} + A_2 \eta^3 \frac{3y^2 - 1}{r_2^3} \tag{29}$$

where $\eta = \frac{R_0}{2H}$, $r_2 = \sqrt{1 + 2\eta rx + \eta^2 r^2}$, and $y = \frac{(1 + \eta rx)}{r_2}$.

Expanding Eq. (29) with respect to η, the coefficients A_1, A_2, are given by

$$A_1 = \frac{1}{2} + \frac{1}{2}\eta^3, \quad A_2 = -\frac{1}{2}\eta^4 \tag{30}$$

while for Eq. (28), the coefficients are

$$A_1' = R_0^3\left(\frac{1}{2} + \frac{1}{2}\eta^3\right), \quad A_2' = -R_0^4\left(\frac{1}{2}\eta^4\right) \tag{31}$$

The inaccuracy in satisfying the boundary condition is reduced to the order η^6. As one can see, the last term in Eq. (29) is small and can be omitted.

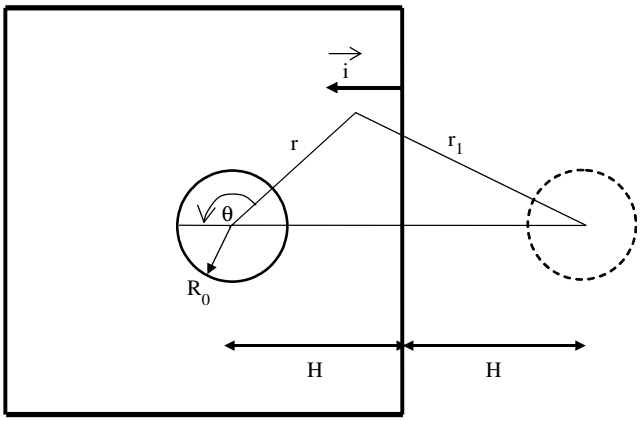

Fig. 3. Particle and its image near a wall.

By substituting Φ given by Eq. (29) into Eqs. (27) and (26), and using the software Maple and Mathematica, one can obtain the following:

$$\alpha = \frac{1}{2} + \mathrm{O}(\eta^3) \tag{32}$$

$$N = -6R_0^2\eta^4 + \mathrm{O}(\eta^7) \tag{33}$$

For monochromatic vibrations of a cell with an amplitude, a, and frequency $\omega = (2\pi f)$, the average of the instantaneous velocity squared over one vibration period is

$$\overline{w^2} = \frac{1}{2}a^2\omega^2 \tag{34}$$

By substituting Eqs. (33) and (34) into Eq. (25), the average attraction force acting on the particle is given by

$$F_{\text{attraction}} = \frac{3}{4}\pi a^2\omega^2\rho_{\mathrm{L}}\left(\frac{\rho_{\mathrm{S}} - \rho_{\mathrm{L}}}{2\rho_{\mathrm{S}} + \rho_{\mathrm{L}}}\right)^2 \frac{R_0^6}{H^4} \tag{35}$$

For a particle of radius R_0 oscillating parallel to a wall, similar calculations yield a slightly different equation for the attraction force as given by

$$F_{\text{attraction}} = \frac{3}{8}\pi a^2\omega^2\rho_{\mathrm{L}}\left(\frac{\rho_{\mathrm{S}} - \rho_{\mathrm{L}}}{2\rho_{\mathrm{S}} + \rho_{\mathrm{L}}}\right)^2 \frac{R_0^6}{H^4} \tag{36}$$

By introducing the dimensionless parameters for the attraction force, fluid density, particle–wall distance, and cell amplitude as follows:

$$\tilde{\rho} = \frac{\rho_{\mathrm{S}}}{\rho_{\mathrm{L}}}, \quad \widetilde{H} = \frac{H}{R_0}, \quad \tilde{a} = \frac{a}{R_0}, \quad \widetilde{F}_{\text{attraction}} = \frac{F_{\text{attraction}}}{\rho_{\mathrm{L}} a\omega^2 V}$$

the above Eqs. (35) and (36) can be written respectively in dimensionless form as

$$\widetilde{F}_{\text{attraction}} = \frac{9}{16}\tilde{a}\left(\frac{\tilde{\rho} - 1}{2\tilde{\rho} + 1}\right)^2\left(\frac{1}{\widetilde{H}^4}\right) \tag{37}$$

$$\widetilde{F}_{\text{attraction}} = \frac{9}{32}\tilde{a}\left(\frac{\tilde{\rho} - 1}{2\tilde{\rho} + 1}\right)^2\left(\frac{1}{\widetilde{H}^4}\right) \tag{38}$$

The variations of the attraction force in Eqs. (37) and (38) are shown in Fig. 4. It is seen clearly that in both cases the dimensionless attraction force decreases with the particle–wall distance to particle radius ratio, $\widetilde{H}$.

As mentioned in the experimental section, it was much easier to measure the shift in the mean position of the particle towards the nearest wall when the particle was oscillating in parallel with rather than normal to the nearest cell wall. Hence, in order to verify Eq. (36), a shift in the plane of the particle oscillation was measured before, during and after the cell was vibrated in the present experiments. The measured shift in the plane of oscillation will be compared to the value predicted from a force balance performed on the particle as shown in Fig. 5. For a particle suspended by a wire, the relation between the attraction force and the shift in the plane of oscillation from the vertical, X_{D}, would be given by

$$F_{\text{attraction}} = (\rho_{\mathrm{S}} - \rho_{\mathrm{L}})gV\frac{X_{\mathrm{D}}}{L} \tag{39}$$

where $\frac{X_{\mathrm{D}}}{L}$ is the sine of the angle of the wire from the vertical, L is the distance from the suspension point to the center of mass of the particle, and V is the volume of the particle. Hence, the particle drift, X_{D}, is given by

$$X_{\mathrm{D}} = \frac{3}{4\pi R_0^3}F_{\text{attraction}}\frac{L}{g(\rho_{\mathrm{S}} - \rho_{\mathrm{L}})} \tag{40}$$

Substituting Eq. (36) into (40) yields

$$X_{\mathrm{D}} = \frac{9}{32}\frac{L}{g}a^2\omega^2\rho_{\mathrm{L}}\frac{\rho_{\mathrm{S}} - \rho_{\mathrm{L}}}{(2\rho_{\mathrm{S}} + \rho_{\mathrm{L}})^2}\frac{R_0^3}{H^4} \tag{41}$$

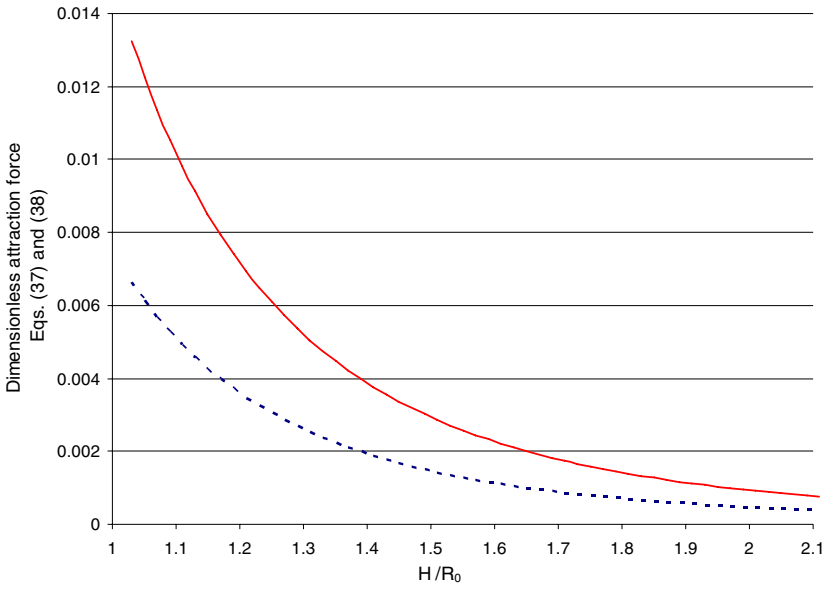

Fig. 4. Variation of the dimensionless attraction force given by Eqs. (37) and (38) – with the particle–wall distance to particle radius ratio, H/R_0, for steel particle in water (cell amplitude = 1.0 mm, particle radius = 6.35 mm).

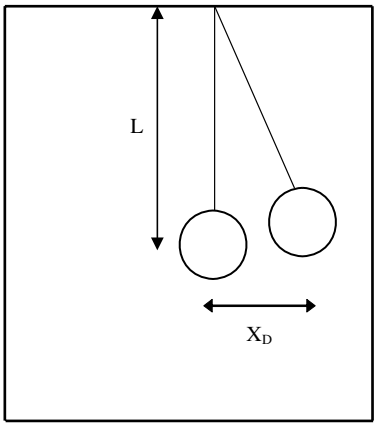

Fig. 5. Shift in the mean position of a particle oscillating parallel to the nearest cell wall and normal to the plane shown.

The predicted drift in the oscillation plane from the vertical will be compared with the experimentally measured values in a later section.

4. Alternate analysis of particle drift near a cell wall

In an alternate analysis, the motion of a spherical particle of diameter R_0 attached to a wire with the point of suspension fixed at a distance H from the nearest wall has been investigated. We assume that the other walls of the fluid cell are sufficiently far from the oscillating particle that their influence can be neglected. We also neglect the influence of the viscosity on the particle motion, which is valid if the Stokes number,

$$S = \frac{1}{R_0}\sqrt{\frac{v}{\omega}} \ll 1 \tag{42}$$

where v and ω are the fluid kinematic viscosity and the cell vibration frequency, respectively.

For the description of the particle dynamics in an inviscid fluid, one can use a Lagrange approach described by the following equation:

$$\frac{\mathrm{d}}{\mathrm{d}t}\left(\frac{\partial L}{\partial \dot{q}_i}\right) - \left(\frac{\partial L}{\partial q_i}\right) = 0 \tag{43}$$

Here q_i is the generalized coordinate required to describe the particle motion, and L is the Lagrange function given by

$$L = T - U \tag{44}$$

where T is the particle kinetic energy and U is its potential energy.

Using Eq. (43) to derive the particle motion, the kinetic energy and the potential energy of the particle have to be calculated. The kinetic energy, T, of the particle in Cartesian coordinates is given by

$$T = \frac{1}{2}A(\dot{x}^2 + \dot{z}^2) + \frac{1}{2}B\dot{y}^2 \tag{45}$$

where z is the vertical coordinate, y is the distance from the particle center of mass to the vertical wall, and x is the horizontal coordinate parallel to the wall (see Fig. 6). The dot above the coordinates x, y and z denotes their derivatives with respect to time, t. The coefficients A and B contain the fluid phase kinetic energy associated with the disturbance flow and are functions of y. If the distance between the particle's center of mass and the nearest wall is substantially smaller than the particle radius, R_0, then the coefficients A and B can be represented in the form of fast converging series in $\frac{R_0}{y}$. The first two terms of this expansion are given in Lamb (1945) and have the following form:

$$A = A(y) = m\left(1 + \frac{1}{2}\varepsilon\left(1 + \frac{3}{16}\frac{R_0^3}{y^3}\right)\right) \tag{46}$$

$$B = B(y) = m\left(1 + \frac{1}{2}\varepsilon\left(1 + \frac{3}{8}\frac{R_0^3}{y^3}\right)\right) \tag{47}$$

where $\varepsilon = \frac{\rho_L}{\rho_S}$ is the density ratio between the fluid and particle, and m is the mass of the particle.

The potential energy of the particle is a sum of two terms related to the gravity field and inertia force field, respectively:

$$U = -m(1-\varepsilon)gL\cos\alpha_n + m(1-\varepsilon)a\omega^2 L\sin\alpha_n \sin\omega t \tag{48}$$

where α_n is the inclination angle between the wire attached to the particle and the equilibrium vertical position, and a is the cell amplitude, as shown in Fig. 6.

The particle in a fluid cell shown in Fig. 6 is subjected to harmonic oscillations normal to the nearest cell wall I. In this paper, a full detail of the derivation will be shown only for the normal vibration case; similar

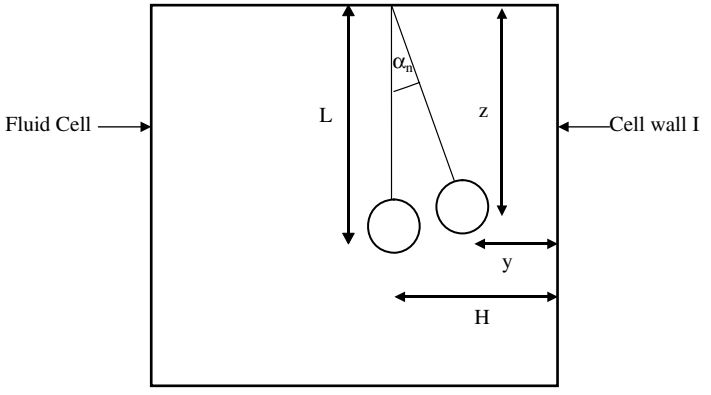

Fig. 6. Particle coordinates near a wall .

calculations are available for the cell motion parallel to the nearest cell wall but only the final expressions derived will be given in this section.

For cell vibrations normal to the nearest cell wall, $x = 0$, and y and z are expressed in terms of the angle of pendulum inclination from the vertical position as

$$y = H - L\sin\alpha_n, \quad z = L\cos\alpha_n \tag{49}$$

Writing down the Lagrange function (43) through α and $\dot{\alpha}$ as

$$\frac{\mathrm{d}}{\mathrm{d}t}\left(\frac{\partial L}{\partial \dot{\alpha}_\mathrm{n}}\right) - \left(\frac{\partial L}{\partial \alpha_\mathrm{n}}\right) = 0 \tag{50}$$

and substituting Eqs. (46)–(49) into (50) yield,

$$\dot{M} = L^2(A-B)\sin\alpha_\mathrm{n}\cos\alpha_\mathrm{n}\dot{\alpha}_\mathrm{n}^2 - \frac{1}{2}L^3(A'\sin^2\alpha_\mathrm{n} + B'\cos^2\alpha_\mathrm{n})\cos\alpha_\mathrm{n}\dot{\alpha}_\mathrm{n}^2 - m(1-\varepsilon)gL\sin\alpha_\mathrm{n} - m(1-\varepsilon)a\omega^2 L\cos\alpha_\mathrm{n}\sin\omega t \tag{51}$$

where

$$M = L^2(A\sin^2\alpha_n + B\cos^2\alpha_n)\dot{\alpha}_n \tag{52}$$

is the angular momentum, and A' and B' are the derivatives of A and B with respect to y.

The above system of equations is non-linear and cannot be solved analytically. However, it can be easily solved numerically for specific values of the parameters involved. As an illustration we plot in Fig. 7 the particle position in horizontal direction predicted as a function of time for the parameter values which correspond to the present experiments (a steel particle in water, $D_\mathrm{p} = 12.7$ mm, $L = 76$ mm, $f = 10$ Hz, and cell amplitude $= 0.88$ mm). To eliminate the influence of initial conditions, the calculations were performed by introducing weak dissipation into the system.

Since the cell vibration amplitudes and consequently the amplitudes of particle oscillations are small we can simplify the equation of particle motion by retaining the non-linear terms of the order not higher than the second order with respect to α. As a result, the following equations can be obtained:

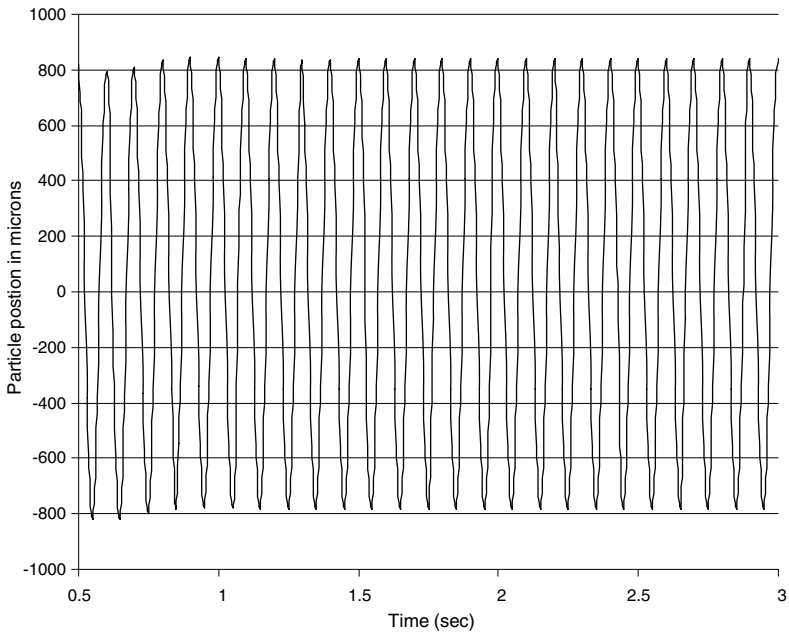

Fig. 7. Numerical solution of Eq. (53) for the particle motion near a wall.

$$\dot{M} = -\frac{1}{2}L^3 B' \dot{\alpha}_n^2 - m(1-\varepsilon)gL\alpha_n - m(1-\varepsilon)a\omega^2 L\left(1 - \frac{1}{2}\alpha_n^2\right)\sin\omega t \tag{53}$$

$$M = L^2 B\dot{\alpha}_n - L^3 B'\alpha_n\dot{\alpha}_n \tag{54}$$

where B and B' are calculated at $y = H$.

We can apply an averaging method to this equation. For that we represent α_n in the form $\alpha_n = \bar{\alpha}_n + \tilde{\alpha}_n(t)$, where $\bar{\alpha}_n$ and $\tilde{\alpha}_n$ are the average and pulsational components of α_n. Retaining only the leading terms in Eqs. (53) and (54), and then solving the above two equations for $\tilde{\alpha}$, one can obtain the following:

$$\tilde{\alpha}_n = C_n \sin\omega t \tag{55}$$

where the constant C_n is given by

$$C_n = \frac{m(1-\varepsilon)a\omega^2}{LB\omega^2 - m(1-\varepsilon)g} \tag{56}$$

The constant C_n is dependent on the physical characteristics of the fluid and particle, the particle diameter, and the distance between the particle center of mass and the nearest wall, H.

By substituting Eq. (55) into Eq. (53) and averaging over a vibration period, the following formula for $\bar{\alpha}_n$ can be obtained:

$$\bar{\alpha}_n = \left(\frac{1}{2m(1-\varepsilon)}\right)\left(\frac{C_n^2 L^2\omega^2 B'}{a\omega^2 C - 2g}\right) \tag{57}$$

The above Eqs. (55) and (57) are not limited to large particle-to-nearest wall distances. If the derivative of B from Eq. (47) at $y = H$ is substituted, the average drift for the case of the particle oscillating normal to the nearest cell wall is given by

$$\bar{\alpha}_n = \left(\frac{9}{32H^4(1-\varepsilon)}\right)\left(\frac{R_0^3 C_n^2 L^2\omega^2\varepsilon}{2g - a\omega^2 C_n}\right) \tag{58}$$

Similar calculations for the case of a particle oscillating parallel to the nearest wall lead to the formulas for the average and pulsational components, $\tilde{\alpha}_p$ and $\bar{\alpha}_p$, given by Eqs. (55)–(58) with B and B' replaced by A and A', respectively. The expressions for these components are then given by

$$\tilde{\alpha}_p = C_p \sin\omega t \tag{59}$$

$$\bar{\alpha}_p = \left(\frac{9}{64H^4(1-\varepsilon)}\right)\left(\frac{R_0^3 C_p^2 L^2\omega^2\varepsilon}{2g - a\omega^2 C_p}\right) \tag{60}$$

where the constant C_p is

$$C_p = \frac{m(1-\varepsilon)a\omega^2}{LA\omega^2 - m(1-\varepsilon)g} \tag{61}$$

Finally, converting the angle to a distance, Eqs. (58) and (60) give respectively

$$X_n = \left(\frac{9}{32H^4(1-\varepsilon)}\right)\left(\frac{R_0^3 C_n^2 L^3\omega^2\varepsilon}{2g - a\omega^2 C_n}\right) \tag{62}$$

$$X_p = \left(\frac{9}{64H^4(1-\varepsilon)}\right)\left(\frac{R_0^3 C_p^2 L^3\omega^2\varepsilon}{2g - a\omega^2 C_p}\right) \tag{63}$$

One can readily show that at high frequencies, Eq. (63) reduces to Eq. (41).

Fig. 8 shows the difference between the mean values of the particle drift predicted for normal and parallel particle oscillations with respect to the nearest wall. As evident from a comparison of Eqs. (62) and (63) shown in Fig. 8, the mean particle drift in the case of the particle oscillating normal to the nearest wall is twice the mean drift of the particle oscillating parallel to the same wall.

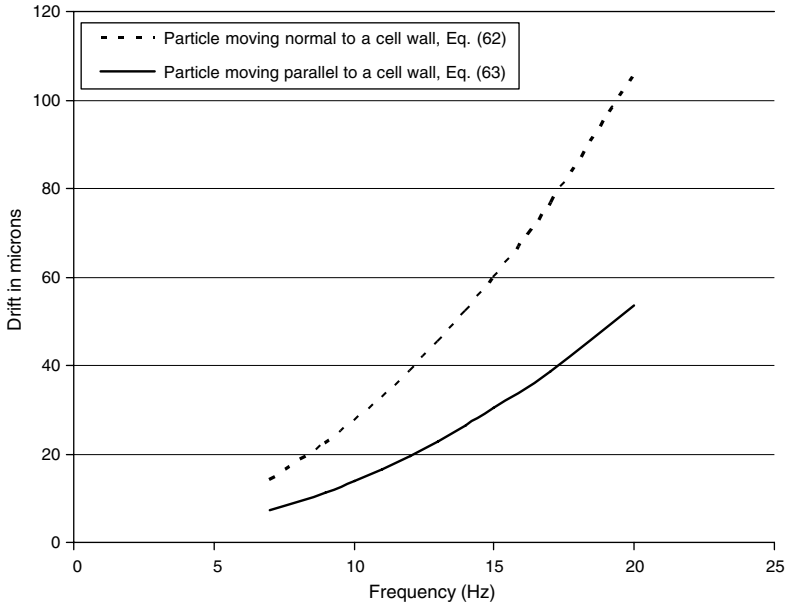

Fig. 8. Comparison of theoretical mean drift for a particle oscillating normal and parallel to a cell wall (a steel particle in water, cell amplitude = 1 mm, $L = 76$ mm, $H = 8.0$ mm before cell vibration, particle diameter = 12.7 mm).

5. Results and discussion

In the experiments involving a particle oscillating normal to the nearest wall, the particle motion was recorded by a 125 fps video camera and the position of the particle was determined as a function of time by analyzing consecutive frames of video images. Fig. 9 shows the particle trajectory and the relative cell wall location when the 12.7 mm diameter steel particle was oscillating at the center of the cell ($H = 25.0$ mm) at a cell vibration frequency of 10 Hz and amplitude of 1.0 mm. The mean position of the particle was unchanged before, during, and after the vibration of the cell.

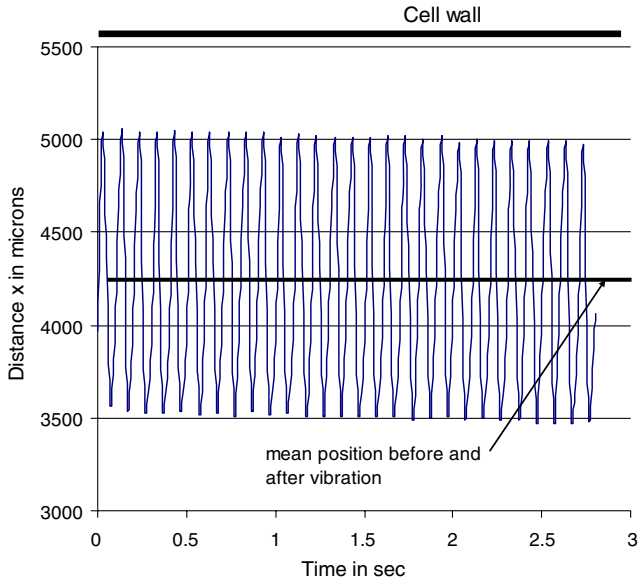

Fig. 9. Variation of particle position with time for cell vibration frequency of 10 Hz and amplitude of 1.0 mm (a steel particle in water placed in the center of the cell).

Table 1
Mean particle drift predicted by Eq. (41) for different cell vibration conditions: constant cell acceleration of 0.4 g using an air-bearing translation stage, $H = 6.7$ mm

Frequency (Hz)	7	8	9	10	12	15	17	20
Cell amplitude (mm)	2.03	1.55	1.23	0.99	0.69	0.44	0.34	0.25
Mean drift (μm)	54	41	33	26	19	12	9	7

Table 2
Mean particle drift predicted by Eq. (41) for different cell vibration conditions: constant cell amplitude of 1.0 mm using a mechanical translation stage, $H = 6.7$ mm

Frequency (Hz)	7	8	9	10	12	15	17	20
Cell acceleration ($\times 10^{-3}$ g)	197	258	326	402	580	906	116	1610
Mean drift (μm)	13	17	22	27	39	61	78	108

In order to verify the attraction force and quantitatively evaluate the wall-proximity effect predicted by the present inviscid models, the predictions of the mean particle drift in a semi-infinite cell given by Eq. (41) or (63) are compared with the experimental data obtained for the steel particle oscillating parallel to the nearest cell wall in a water-filled fluid cell. The particle drift was clearly observed when the particle oscillation was recorded using a video camera situated in the plane of the particle oscillation as shown in Fig. 2. As soon as the cell began vibrating at a sufficiently high frequency, the plane of the particle oscillation drifted towards the nearest wall due to the attraction force and reached a new equilibrium position which remained stationary during the cell vibration. After the cell vibration was stopped, the plane of the particle oscillation returned to its initial vertical position. Experimentally, the drift could be detected only above a cell vibration frequency of 9 Hz, and increased with the cell vibration frequency.

The theoretical predictions of the mean particle drift given by Eq. (41) are shown for different cell vibration frequencies in Tables 1 and 2, for a constant cell acceleration level of 0.4 g and a constant cell amplitude of 1.0 mm, respectively.

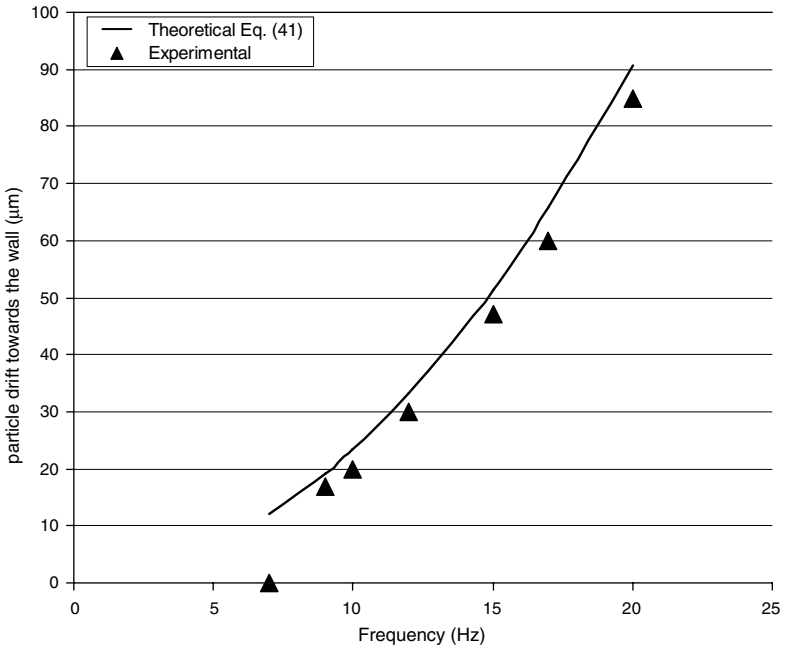

Fig. 10. Variation of the particle drift with the cell frequency for a steel particle in water: cell amplitude = 1.0 mm, $L = 76$ mm, $H = 7.0$ mm before cell vibration, particle diameter = 12.7 mm.

Figs. 10–13 show comparisons of the theoretical and experimental variations in the particle drift with the cell vibration frequency for different distances between the particle and the nearest wall ($H = 7.0$–17.0 mm). For $H = 7.0$ mm, the particle drift due to an attraction force increased from 25 μm at 10 Hz to 55 μm at 15 Hz (Fig. 10). No particle drift was measurable when it was less than 5 μm, and thus no data are shown in Figs. 11–13 for those measurements. At higher frequencies, this drift could be accurately measured and was in close agreement with the theoretical predictions of the inviscid model Eq. (41).

Figs. 11 and 12 show the particle drift data and predictions for larger particle-to-wall distances of $H = 9.0$ mm and 11.0 mm. Compared to the $H = 7.0$ mm data, the values of particle drift are smaller and decreased with increasing H. When the particle-to-wall distance was increased to 17.0 mm, no drift could be measured in the plane of the particle oscillation as shown in Fig. 13. In all cases, there is good agreement between the experimental results and the inviscid model predictions of Eq. (41), for sufficiently small values of H.

Although not systematically investigated experimentally, the fluid and particle densities have significant influences on the vibration-induced attraction force. In the presence of air in the fluid cell instead of water, an oscillating steel particle showed no drift in the mean position under the same vibration conditions, even

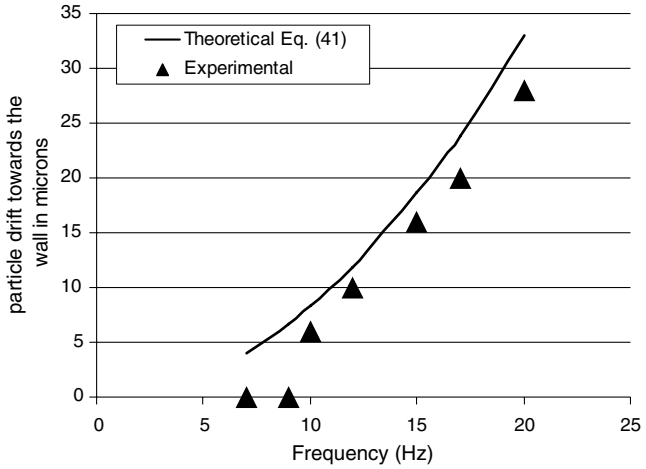

Fig. 11. Variation of the particle drift with the cell frequency for a cell amplitude of 1.0 mm: a steel particle in water, $L = 76$ mm, $H = 9.0$ mm before cell vibration, particle diameter = 12.7 mm.

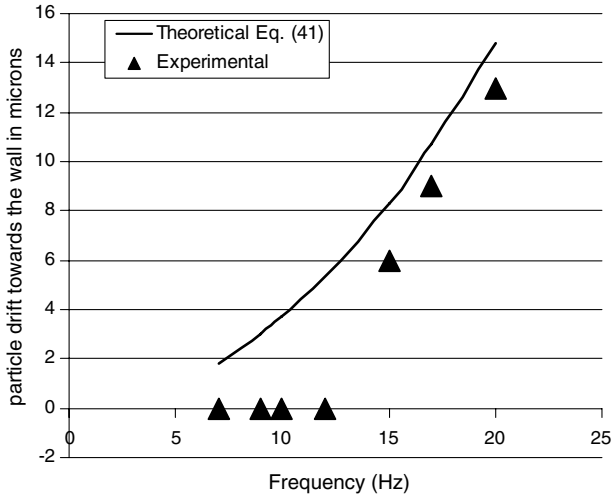

Fig. 12. Variation of the particle drift with the cell frequency for a cell amplitude of 1.0 mm: a steel particle in water, $L = 76$ mm, $H = 11.0$ mm before cell vibration, particle diameter = 12.7 mm.

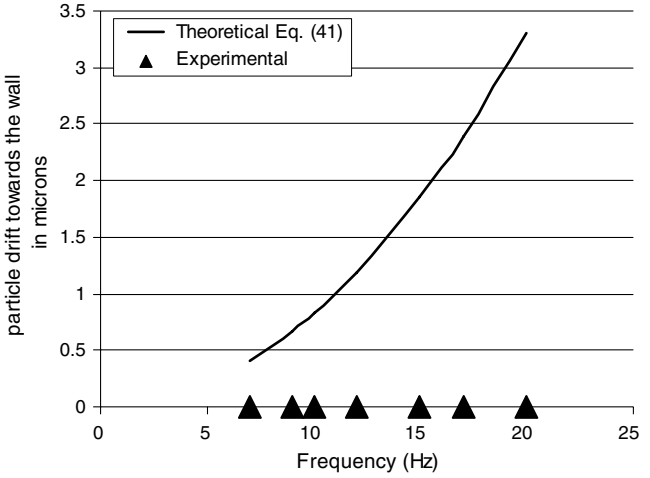

Fig. 13. Variation of the particle drift with the cell frequency for a cell amplitude of 1.0 mm: a steel particle in water, $L = 76$ mm, $H = 16.0$ mm before cell vibration, particle diameter = 12.7 mm.

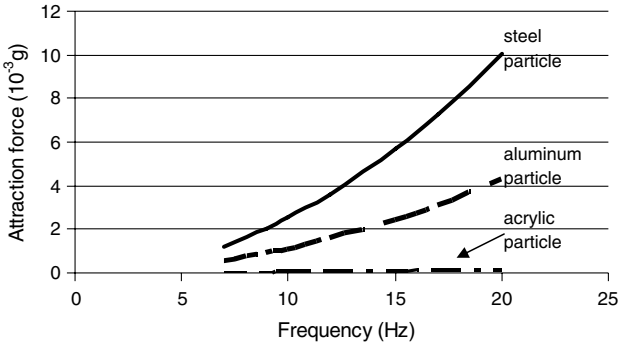

Fig. 14. Theoretical variation of the attraction force with cell frequency for different particle densities (cell amplitude = 1.0 mm, $L = 76$ mm, $H = 8.0$ mm before cell vibration, particle diameter = 12.7 mm).

if the particle and the wire were placed near one of the cell walls. For very small fluid densities, the attraction force would be negligibly small as given by Eq. (36).

Eqs. (35) and (36) also predict a strong effect of particle density on the attraction force when the fluid density is kept constant. Fig. 14 shows the variations of the attraction force for a particle oscillating normal to the nearest cell wall (Eq. 35) with the cell vibration frequency for different particle densities. For solid particles under microgravity and without any wire attached, cell vibration due to g-jitter would cause not only an oscillating motion, but also a gradual drift in the mean position towards the nearest wall. Although the attraction force may be quite small for particles having a similar density as that of the surrounding fluid such as a protein crystal, the vibration-induced attraction force would cause the particle to drift over a significant distance within the fluid cell under microgravity given enough time which is typically required for protein crystal growth.

6. Conclusion

The vibration-induced attraction force on a particle oscillating near a wall in a fluid cell has been investigated experimentally and theoretically. The particle motion was investigated experimentally by suspending a spherical steel particle by a thin wire in a fluid cell and vibrating the cell horizontally at different frequencies and amplitudes. When the particle was oscillating in the center of the cell sufficiently far away from all the cell

walls, the mean particle position was unaffected before, during, and after the vibration of the cell at all vibration frequencies. But when the particle suspended by a wire was oscillating near one of the cell walls, there was a clear shift in the particle mean position towards the nearest cell wall due to the attraction force. For both cases of particle oscillation normal to and parallel with the nearest wall, the drift in the mean particle position increased with the cell vibration frequency and amplitude, and decreased with the distance between the particle center of mass and the nearest wall.

Theoretical models of the attraction force and its effect on the mean position of the oscillating particle were developed assuming an inviscid fluid. Analytical expressions were derived for the attraction force and the magnitude of the drift in the particle mean position for a particle suspended by a wire in a fluid cell and oscillating near a cell wall. The model predictions were seen to be in good agreement with the experimental data obtained for a steel particle oscillating parallel with the nearest wall in a water-filled cell under various cell vibration conditions.

Acknowledgements

The authors would like to thank the Canadian Space Agency for financially supporting this work, and the Government of Ontario for a graduate fellowship received by S. Hassan.

References

Baird, M.H.I., Senior, M.G., Thompson, R.J., 1967. Terminal velocities of spherical particles in a vertically oscillating liquid. Chem. Eng. Sci. 22, 551–558.

Basset, A.B., 1887. On the motion of two spheres in a liquid and allied problems. Quart. J. 18, 369–377.

Basset, A.B., 1888A Treatise on Hydrodynamics, 2. Deighton, Bell and Co, Cambridge (Chapter 21). Also New York: Dover publications, Inc., 1961.

Boussinesq, J.V., 1885. Sur la Resistance qu'oppose un Liquide Indefeni au Repos sans Pesanteur, au Mouvememt d'une Sphere Solide qu'il Mouille sur toute sa Surface. C. R. des Séances de l'Academie 100, 935–937.

Chelomey, V.N., 1983. Paradoxes in mechanics caused by vibrations. Akad. Nauk. SSSR. 270, 62–67.

Clift, R., Grace, J.R., Weber, M.E., 1978. Bubbles, Drops and Particles. Academic Press Inc., London.

Eames, I., Hunt, J.C.R., Belcher, S.E., 1996. Displacement of inviscid fluid by a sphere moving away from a wall. J. Fluid Mech. 324, 333–353.

Happel, J., Brenner, H., 1983. Low Reynolds Number Hydrodynamics. Kluwer Acad. Publishers, Dordrecht, The Netherlands.

Hassan, S., Kawaji, M., Lyubimova, T.P., Lyubimov, D.V., 2006a. Motion of a sphere suspended in a vibrating liquid-filled container. ASME J. Appl. Mech. 73, 72–78.

Hassan, S., Kawaji, M., Lyubimova, T.P., Lyubimov, D.V., 2006b. The effects of vibrations on particle motion near a wall in a semi-infinite fluid cell. ASME J. Appl. Mech. 73, 610–621.

Hicks, V.M., 1880. On the motion of two spheres in a fluid. Philos. Trans. Roy. Soc. London 171, 454–470.

Houghton, G., 1961. The behaviour of particles in a sinusoidal vector field. Proc. Roy. Soc. A 272, 33–43.

Ikeda, S., Yamasaka, M., 1989. Etude du mouvement d'une sphère dans un liquide pulsé. Fluid Dyn. Res. 5, 203–216.

Jameson, G.J., Davidson, J.F., 1966. The motion of a bubble in a vertically oscillating liquid: theory for an inviscid liquid, and experimental results. Chem. Eng. Sci. 21, 29–33.

Lamb, H., 1945. Hydrodynamics. Cambridge University Press, London.

Leahy, A.H., 1884. On the pulsations of spheres in an elastic medium. In: Proceedings of the Cambridge Philosophical Trans. of the Royal Society of London, vol. 14, pp. 45–62.

Li, L., Schultz, W.W., Merte, H., 1993. The velocity potential and the interacting force of two spheres moving perpendicularly to the line joining their centers. J. Eng. Math. 27, 147–160.

Magnaudet, J., 2003. Small inertial effects on a spherical bubble, drop or particle moving near a wall in a time-dependent linear flow. J. Fluid Mech. 485, 115–142.

Magnaudet, J., Eames, I., 2000. The motion of high Reynolds-number bubbles in inhomogeneous flows. Ann. Rev. Fluid Mech. 32, 659–708.

Milne-Thomson, L.M., 1968. Theoretical hydrodynamics, fifth ed. Macmillan, London.

Molinier, J., Kuychoukov, G., Angelino, H., 1971. Etude du mouvement d'une sphère dans un liquide pulsé. Chem. Eng. Sci. 26, 1401–1412.

Riley, N., 2001. Steady streaming. Ann. Rev. Fluid Mech. 33, 43–65.

Stokes, C.G., 1851. Mathematical and Physical Papers, 3, p. 1.